Combined nanomechanical and nanomagnetic analysis of magnetoelectric memories

S. Giordano, Yannick Dusch, Nicolas Tiercelin, Philippe Pernod, Vladimir Preobrazhensky

Combined nanomechanical and nanomagnetic analysis of magnetoelectric memories

Stefano Giordano,[1,*] Yannick Dusch,[1] Nicolas Tiercelin,[1] Philippe Pernod,[1] and Vladimir Preobrazhensky[1,2]
[1]*International Associated Laboratory LEMAC: IEMN, UMR CNRS 8520, PRES Lille Nord de France, ECLille, 59651 Villeneuve d'Ascq, France*
[2]*Wave Research Center, Prokhorov General Physics Institute, Russian Academy of Science, 38 Vavilov str., Moscow 119991, Russia*
(Received 14 March 2012; published 25 April 2012)

Magneto-electro-elastic and multiferroic materials can be combined in appealing nanostructures characterized by the coexistence and coupling of electric, magnetic, and mechanical phases with potential applications in novel multifunctional devices. Here, we derive a theory for nonvolatile room-temperature memory elements composed of magnetostrictive nanoparticles embedded in a piezoelectric matrix: two stable orthogonal magnetization states are obtained by the competition of anisotropy and external magnetic polarization. The innovative nontoggle switching between the states is modeled by a thorough combination of the nanomechanical Eshelby approach with the nanomagnetic Landau-Lifshitz-Gilbert formalism, yielding a robust picture of the dynamical behavior and allowing the improvement of the energetic efficiency.

DOI: 10.1103/PhysRevB.85.155321 PACS number(s): 75.80.+q, 62.25.−g, 85.75.−d, 85.80.Jm

I. INTRODUCTION

Magneto-electro-elastic and multiferroic heterostructures have become one of the hottest topics of condensed matter physics in recent years.[1–5] The coexistence of electric, magnetic, and elastic subsystems brings out novel physical phenomena and offers possibilities for new devices, such as sensors, actuators, transducers, and memories.[6] Of paramount interest is the cross coupling between the magnetic and electric orders. In fact, the magnetic field control of electric polarization and the electric field control of magnetization have been observed in different materials.[7,8] However, because of the weak magnetoelectric coupling of most single-phase systems, the introduction of composites, such as ferromagnetic-ferroelectric heterostructures, offers a promising route for obtaining strong cross couplings. In these structures, the coupling between polarization and magnetization is mechanically mediated through the magnetostrictive and the piezoelectric properties of the components. Typically, the heterogeneous structure is multilayered or composed of a ferromagnetic nanoparticle in contact with or embedded into a ferroelectric substrate or matrix.[5] The determination of the exact distribution of the elastic fields in the structure is crucial for quantifying the coupling between the ferroic phases. Therefore the nanomechanical techniques,[9] e.g., based on the multiphysics Eshelby theory,[10] are of primary importance and must be combined with ferromagnetic[11,12] and/or ferroelectric[13] models in order to obtain the whole picture of the heterostructures behavior.

One of the most important reasons for considering multiferroic materials and structures comes from the global demand for low-power devices. In fact, it is generally accepted that the factor limiting the down scaling and the high integration level in standard semiconductor electronics is the power dissipation.[14] The energy needed for switching the state of a bit in a standard electronic device is equal to at least $Nk_BT\ln(1/p)$, where N is the numbers of electrons (weakly or noninteracting carriers) involved in the process, k_B is the Boltzmann constant, T is the temperature and p is the bit error probability. On the other hand, if the information is encoded in the magnetization state of a monodomain ferromagnet (with M strongly interacting spins), the switching process dissipates an energy equal to about $k_BT\ln(1/p)$, independently of the number M of spins.[15] Because of this remarkable result, ferromagnetic and multiferroic nanolayers and nanoparticles are attracting increasing attention for computing architectures and for systems based on energy harvesting techniques.[16,17] In particular, mechanically induced rotation of magnetization consumes extremely low energies and is very appropriate for nanomagnetic logic.[18,19]

Among all the above mentioned applications, multiferroic or magnetoelectric random access memories (RAM) are paradigmatic examples promising nonvolatile magnetic storage and low power consumption. In these devices, the information is stored in different magnetization states of a ferromagnetic phase and the switching is controlled by electric and/or elastic actions. The exploiting of single-phase multiferroic barriers into magnetic tunneling junctions allowed the implementation of memory cells, but still far below room temperature.[20] Also the direct control of magnetization by electric field is achieved at very low temperatures in GaMnAs semiconductors.[21,22] For practical applications, the weak magnetoelectric interactions of room temperature multiferroics such as bismuth ferrite ($BiFeO_3$) or chromium oxide (Cr_2O_3) can be amplified using specific interfacial properties, but this approach requires high-quality crystals and interfaces.[23–25]

Besides intrinsic multiferroics, several multiphase heterostructures have been proposed in order to control the memory effect with electric and elastic external fields.[26–28] However, difficulties in precisely controlling the local magnetization switching and in obtaining the nonvolatile requirement induced further researches. Of particular interest are the solutions based on a temporary magnetic anisotropy induced by a pulse of electric field. In fact, controlled pulses allow the magnetization switching between two opposite states.[29–31] Detailed and refined simulations have been recently performed to evaluate the performances of this technique.[32] It allows a 180° "ballistic switch" of the magnetization, but still presents some limitations: (i) for symmetry reasons, the system is a toggle memory, which means that the state of the system must be known prior writing new information, and (ii) since it relies on precession of the magnetization toward the new state after

the electric pulse, it implies a very precise control of this pulse in the subnanosecond time scale.

To circumvent these issues, we suggest to spatially break the symmetry of the equilibrium positions. This point can be simply realized by considering two orthogonal magnetization states.[33] In this paper, we are concerned with this approach, here implemented in a new paradigmatic (nontoggle and nonvolatile) memory structure. We suppose to introduce a magnetostrictive nanoparticle into a piezoelectric matrix. In this structure, it is possible to obtain two orthogonal stable positions of the magnetization generated by the competition between anisotropic and Zeeman energies.[33–35] The action of the piezoelectric matrix, coupled with the magnetostriction of the particle, is able to yield (i) a nontoggle switching between the states of the memory (it means that it is possible to write new information without the knowledge of the stored bit) and (ii) a commutation process that does not depend on the shape and on the timing of the applied electric pulse.

The present investigation is relevant from the technological point of view because of the proposed innovative structure. On the other hand, a continuum model is here developed, fully describing the physics of the system in both static and dynamic regimes. In fact, for studying particle/matrix heterostructures, we develop a general and versatile procedure based on the combination of the Eshelby nanomechanical method[9,10] with the Landau-Lifshitz-Gilbert (LLG) nanomagnetism formalism.[11,12]

We have chosen a geometry based on an ellipsoidal particle embedded in a matrix for two main reasons: firstly, the choice of a particle makes possible the large-scale integration in a planar array of elements, and secondly, it is well known that the physical fields, induced within an ellipsoidal inhomogeneity by remotely applied sources, are always uniform assuring the easy control of the internal magnetization. However, the determination of the internal fields in an ellipsoidal particle from the externally applied ones requires a refined theory based on the Eshelby formalism, generalized in order to consider the electro-magneto-elastic coupling.[9,10] The thorough analysis of the elastic fields is crucial for evaluating the magnetoelectric interaction, which is mediated by the mechanical stress distributed over the particle-matrix interface. Hence, we developed the complete theoretical procedure for determining all the electromagnetic and mechanical fields in the structures. In particular, it predicts the existence of two stable magnetization states and allows us to define the switching scheme, controlled by the piezoelectric matrix. Then, this first theoretical device was combined with the LLG equation, which is able to describe the dynamic behavior of the magnetization vector within the particle.[11,12] We therefore studied the intriguing and complex dynamic scenario framing the time evolution of the magnetization in a ferromagnetic nanoparticle embedded in the piezoelectric matrix. It is important to observe that only a given range of values for the electric field is appropriate for obtaining a correct switching behavior. This point is strongly related to the complicated and tortuous three-dimensional trajectories followed by the magnetization during the dynamical phases. Finally, we established a robust picture of the commutation strategy, we performed the energetic analysis and we determined the switching times of the device.

The structure of the paper is the following. In Sec. II, we introduce the memory element constituted of the ferromagnetic particle embedded into the piezoelectric matrix and we define the theoretical formalism used for its description. In Secs. III and IV, we analyze in detail the coupling with the externally applied magnetic and electro-mechanic fields, respectively. Here, we make extensive use of the multiphysics Eshelby theory. In Sec. V, we summarize the set of equations describing the memory element and we obtain the static behavior of the system. In particular, we prove the possibility to obtain the bistable character of the magnetization with two orthogonal orientations. In Sec. VI, we apply the LLG equation to describe the dynamic response of the system. We demonstrate the thermal stability, the high switching rapidity, and the energetic efficiency of the device.

II. THE MEMORY ELEMENT

We briefly introduce here the principle of operation of the memory element. We take into consideration a magnetoelastic particle embedded in a piezoelectric matrix, as represented in Fig. 1. The particle shows two kinds of anisotropy: the geometrical one, caused by the prolate shape of the ellipsoid, and the physical one, induced through technological processes. Both of them tend to align the magnetization along the x axis (without any preference between positive and negative directions). We now propose to apply a magnetic field along the y axis. From the technological point of view, this field can be obtained, for example, through a permanent nanomagnet. The competition between the anisotropy and the applied magnetic field generates two energetically equivalent stable orientations for the magnetization. They are represented by the quite orthogonal red and blue arrows in Fig. 1. Of course, to obtain an usable memory element, we must be able to switch the magnetization between these states with a reversible and versatile mechanism. To do this, we take advantage of the magnetostriction of the particle coupled with the piezoelectric matrix. In fact, the magnetostrictive ellipsoid exhibits two

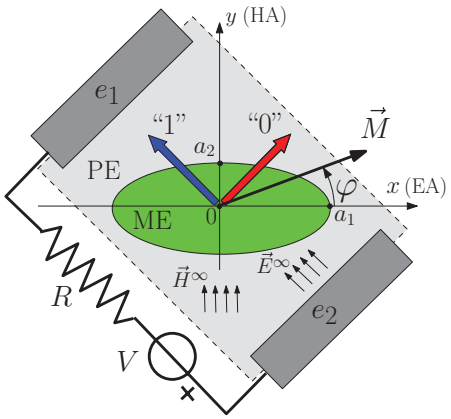

FIG. 1. (Color online) Scheme of the magnetoelastic (ME) particle embedded in the piezoelectric (PE) matrix. The easy axis (EA) and the hard axis (HA) of the particle are aligned with the reference frame (x, y). The electrodes e_1 and e_2 generate the electric field $\vec{E}^\infty$ at $\varphi = 3\pi/4$ while the magnetic field $\vec{H}^\infty$ is applied at $\varphi = \pi/2$. The resulting two stable positions for $\vec{M}$ correspond to the values "0" and "1" of the stored bit.

properties: (i) when magnetized, it changes its shape extending in the direction of the magnetization and shrinking in the orthogonal plane, and (ii) conversely, when arbitrarily strained, the resulting magnetization tends to align with the direction of the larger elongation. We can exploit this latter property as follows: a varying (positive or negative) electric field applied to the system generates, through the piezoelectric effect, a tensile or compressive stress along the direction at $\varphi = 3\pi/4$ (see Fig. 1). Independently of the initial state of the memory, a tensile stress leads to the recording of the bit "1," while a compressive stress leads to the bit "0." We have therefore obtained a nontoggle switching mechanism, which will be thoroughly modeled in the following. The reading of the recorded state can be realized through the magnetoresistance property in a magnetic tunneling junction (vertically assembled on the memory element).[36]

To be concrete, we consider the ellipsoidal nanoparticle depicted in Fig. 1 made of $TbFe_2$ (terfenol) with the following dimensions: $2a_1 = 45$ nm along x, $2a_2 = 25$ nm along y, $2a_3 = 20$ nm along z. We suppose that the size of the particle is small enough to assure that the particle can be treated as a single ferromagnetic domain: a uniform magnetization $\vec{M} = M_s\,\vec{\gamma}$ appears, where $M_s = 64 \times 10^4$A/m is the magnetization at saturation and $\vec{\gamma}$ is a unit vector. The first aim of the following procedure is that of determining the orientation $\vec{\gamma}$ in terms of the externally applied fields and of the environment where the particle is embedded. It can be obtained by minimizing the energy function as follows:[37]

$$w(\vec{\gamma}) = -\mu_0 M_s \vec{\gamma}\cdot\vec{H} + \varphi_a(\vec{\gamma}) - \hat{T} : \hat{\varepsilon}_\mu(\vec{\gamma}). \tag{1}$$

The first term represents the Zeemann energy and describes the influence of the local magnetic field $\vec{H}$ on the orientation of $\vec{\gamma}$. The second term $\varphi_a(\vec{\gamma})$ represents the anisotropic energy. It is possible to induce in $TbFe_2$ an uniaxial anisotropy that tries to align the magnetization along the x direction, called easy axis, EA (on the other hand, the y direction is named hard axis, HA). Therefore we have an anisotropic energy $\varphi_a(\vec{\gamma}) = -(1/2)\mu_0 M_s H_a \gamma_x^2$ where it is possible to get an effective magnetic field $H_a = 18 \times 10^4$A/m.[33,38] The third term represents the elastic interaction energy, where $\hat{T}$ is the local stress tensor and $\hat{\varepsilon}_\mu(\vec{\gamma})$ is the strain tensor induced by the magnetization (magnetostriction). As terfenol is supposed to be amorphous, the magnetostriction coefficient can be evaluated using $\lambda_{111} = 1.7 \times 10^{-3}$ and $\lambda_{100} = 0.1 \times 10^{-3}$ into the averaging formula $\lambda_s = \frac{3}{5}\lambda_{111} + \frac{2}{5}\lambda_{100} \approx 1.06 \times 10^{-3}$.[39] The corresponding strain is given by $\hat{\varepsilon}_\mu(\vec{\gamma}) = (\lambda_s/2)(3\vec{\gamma}\otimes\vec{\gamma} - \hat{I})$, where $\hat{I}$ is the identity tensor. We can say that w represents the thermodynamic potential of the particle at given $\vec{H}$ and $\hat{T}$.

It is important to remark that the local magnetic field and the local stress tensor enter the energy function as parameters. Therefore the nonlinear minimization furnishes the direction in terms of the magnetic field and the stress tensor:

$$\min_{\vec{\gamma}:\,\|\vec{\gamma}\|=1} w(\vec{\gamma};\vec{H},\hat{T}) \quad\Rightarrow\quad \vec{\gamma} = \vec{\gamma}(\vec{H},\hat{T}). \tag{2}$$

The constitutive equations of the particle follow: from the magnetic point of view, we have

$$\vec{B} = \mu_0(\vec{H} + \vec{M}) = \mu_0[\vec{H} + M_s\vec{\gamma}(\vec{H},\hat{T})], \tag{3}$$

where $\vec{B}$ is the magnetic induction. From the elastic point of view, we have

$$\hat{T} = \hat{L}_2\{\hat{\varepsilon}_0 - \hat{\varepsilon}_\mu(\vec{\gamma})\} = \hat{L}_2\{\hat{\varepsilon}_0 - \hat{\varepsilon}_\mu[\vec{\gamma}(\vec{H},\hat{T})]\}, \tag{4}$$

where $\hat{\varepsilon}_0$ is the local strain tensor (measured with respect to the demagnetized particle) and $\hat{L}_2$ is the stiffness tensor of the particle (it shows an isotropic behavior characterized by the Young modulus $E = 110$ GPa and by the Poisson ratio $\nu = 0.35$).

Finally, we underline that the local magnetic field $\vec{H}$ and the stress tensor $\hat{T}$ inside the particle depend on the environment where the particle is embedded and on the external fields applied to the structure. This point will be treated in the following two sections.

III. COUPLING WITH THE EXTERNAL MAGNETIC FIELD

As stated above, the magnetic field $\vec{H}$ entering the energy function is the local (internal) magnetic field and, therefore, it is important to obtain its relationships with the externally applied magnetic field $\vec{H}^\infty$. To this aim, we can utilize a recent result, which is valid for an arbitrary nonlinear and anisotropic ellipsoidal particle embedded in a linear but anisotropic matrix.[40–42] We consider a nonlinear ellipsoidal inhomogeneity (having semiaxes a_1, a_2, and a_3) described by the (magnetic field dependent) permeability tensor $\hat{\mu}_2 = \hat{\mu}_2(\vec{H})$ embedded in a linear matrix with permeability tensor $\hat{\mu}_1$. In these conditions, we have the implicit equation

$$\vec{H} = \left\{\hat{I} - \hat{S}_m\left[\hat{I} - \hat{\mu}_1^{-1}\hat{\mu}_2(\vec{H})\right]\right\}^{-1}\vec{H}^\infty, \tag{5}$$

where $\hat{S}_m$ is the magnetic Eshelby tensor given by[41]

$$\hat{S}_m = \frac{\det(\hat{a})}{2}\int_0^{+\infty}\frac{(\hat{a}^2 + s\hat{\mu}_1)^{-1}\hat{\mu}_1}{\sqrt{\det(\hat{a}^2 + s\hat{\mu}_1)}}ds. \tag{6}$$

Here, $\hat{a}$ is a tensor defining the geometry of the ellipsoid: $\hat{a} = \mathrm{diag}(a_1,a_2,a_3)$. Interestingly enough, we note that the magnetic Eshelby tensor depends only on the geometry of the system and on the matrix permeability tensor. Equation (5) is implicit and therefore it should be solved in order to find $\vec{H}$ as function of $\vec{H}^\infty$. Using the definition of the nonlinear constitutive equation of the particle $\vec{B} = \hat{\mu}_2(\vec{H})\vec{H} = \mu_0(\vec{H} + \vec{M})$, we can write Eq. (5) in a different form. In our case, the nonlinear behavior is introduced by the arbitrary relation between the magnetization $\vec{M}$ and the local magnetic field $\vec{H}$ [defined through the minimization problem stated in Eq. (1)]. From Eq. (5), we simply obtain

$$\vec{H} - \hat{S}_m\vec{H} + \hat{S}_m\hat{\mu}_1^{-1}\hat{\mu}_2(\vec{H})\vec{H} = \vec{H}^\infty. \tag{7}$$

and, using Eq. (3), we have

$$\vec{H} - \hat{S}_m\vec{H} + \hat{S}_m\hat{\mu}_1^{-1}\mu_0\vec{H} + \hat{S}_m\hat{\mu}_1^{-1}\mu_0 M_s\vec{\gamma} = \vec{H}^\infty. \tag{8}$$

Finally, after straightforward calculations, we obtain

$$\begin{aligned}\vec{H} &= \left[\hat{I} - \hat{S}_m\left(\hat{I} - \hat{\mu}_1^{-1}\mu_0\right)\right]^{-1}\left[\vec{H}^\infty - \hat{S}_m\hat{\mu}_1^{-1}\mu_0 M_s\vec{\gamma}\right]\\ &= \hat{A}\vec{H}^\infty + \hat{N}\vec{\gamma},\end{aligned} \tag{9}$$

where the tensors $\hat{A}$ and $\hat{N}$ can be identified by the first line of Eq. (9). It is not difficult to prove that the tensor $\hat{N}$ is always

symmetric, i.e., $N_{ij} = N_{ji}$. At the end, the local magnetic field has been explicitly written in terms of the remotely applied magnetic field and of the internal magnetization orientation $\vec{H} = \vec{H}(\vec{H}^{\infty}, \vec{\gamma})$. This is the most important achievement of this section.

Equation (9) can be simplified for an isotropic or crystalline cubic matrix. In this case, we have $\hat{\mu}_1 = \mu_1 \hat{I}$, where μ_1 is the scalar permeability and $\hat{I}$ is the identity tensor. Therefore we obtain a simpler version of the magnetic Eshelby tensor $\hat{S}_m = \mathrm{diag}(L_1, L_2, L_3)$, where the L_i's are the so-called depolarization factors[43,44]

$$L_i = \frac{a_1 a_2 a_3}{2} \int_0^{+\infty} \frac{d\eta}{\left(a_i^2 + \eta\right) \prod_{j=1}^{3} \sqrt{a_j^2 + \eta}}. \tag{10}$$

So, the local magnetic field is given by the relation

$$H_i = \frac{\mu_1 H_i^{\infty} - L_i \mu_0 M_s \gamma_i}{(1 - L_i)\mu_1 + L_i \mu_0} \tag{11}$$

controlled by the above defined depolarization factors. Finally, in the more specific case with $\mu_1 = \mu_0$, we obtain the very simple result

$$H_i = H_i^{\infty} - L_i M_s \gamma_i, \tag{12}$$

which is standard in many micromagnetic developments.[45]

IV. COUPLING WITH THE EXTERNAL ELECTRIC AND ELASTIC FIELDS

The coupling with the external electric and elastic fields is mediated by the piezoelectric matrix, where the particle is embedded. We search for the relationship between the local stress $\hat{T}$ and the applied electric field $\vec{E}^{\infty}$ and the remote elastic strain $\hat{\varepsilon}^{\infty}$. We begin this analysis by defining the constitutive equation of the matrix

$$\hat{T} = \hat{L}_1 \hat{\varepsilon} + \hat{Q}_1 \vec{E}, \tag{13}$$

$$\vec{D} = \hat{R}_1 \hat{\varepsilon} + \hat{\epsilon}_1 \vec{E}, \tag{14}$$

where $\hat{L}_1$ is the elastic stiffness tensor, $\hat{\epsilon}_1$ is the permittivity tensor, and $\hat{Q}_1$ and $\hat{R}_1 = -\hat{Q}_1^T$ are the piezoelectric tensors of the matrix. In order to obtain a more compact notation, we define the following generalized tensor variables:

$$\hat{\Sigma} = [\hat{T} | \vec{D}] \quad \text{and} \quad \hat{Z} = \begin{bmatrix} \hat{\varepsilon} \\ \hline -\vec{E} \end{bmatrix}, \tag{15}$$

where $\hat{\Sigma}$ is represented by a matrix 3×4 and $\hat{Z}$ is represented by a matrix 4×3. The piezoelectric matrix behavior can be therefore summarized through the relation

$$\Sigma_{iJ} = (\Lambda_1)_{iJMn} Z_{Mn} \quad \text{or} \quad \hat{\Sigma} = \hat{\Lambda}_1 \hat{Z} \tag{16}$$

where $i,n = 1,2,3$ and $J,M = 1,2,3,4$. The tensor $\hat{\Lambda}_1$ contains all the elastic, dielectric and piezoelectric responses of the matrix. It fulfils the standard symmetry rule $(\Lambda_1)_{iJMn} = (\Lambda_1)_{nMJi}$, which can be derived through energetic considerations. For sake of completeness, such details are discussed in Appendix A.

We observe now that the particle is embedded into the matrix when it has a specific magnetization state identified by an initial direction $\vec{\gamma}_0$ and, consequently, by an initial magnetostriction state identified by $\hat{\varepsilon}_{\mu}(\vec{\gamma}_0)$. We want to measure the local strain with respect to such a configuration and, therefore, we define the local strain as $\hat{\varepsilon} = \hat{\varepsilon}_0 - \hat{\varepsilon}_{\mu}(\vec{\gamma}_0)$. Here, $\hat{\varepsilon}_0$ is the local strain tensor defined in Eq. (4) and it is measured with respect to the demagnetized particle. From the technological point of view, the physical and geometric anisotropy of the particle assures that $\vec{\gamma}_0$ is aligned with the x axis and therefore $\vec{\gamma}_0 = \pm\vec{e}_1$ (where $\vec{e}_i$ is the unit vector along the ith axis). Since the magnetostriction $\hat{\varepsilon}_{\mu}(\vec{\gamma})$ is a quadratic form in $\vec{\gamma}$, we have $\hat{\varepsilon}_{\mu}(\vec{\gamma}_0) = \hat{\varepsilon}_{\mu}(\vec{e}_1) = \hat{\varepsilon}_{\mu}(-\vec{e}_1)$ in our specific case. So, the constitutive equations of the particle in the new reference frame read

$$\hat{T} = \hat{L}_2 \{\hat{\varepsilon} - [\hat{\varepsilon}_{\mu}(\vec{\gamma}) - \hat{\varepsilon}_{\mu}(\vec{\gamma}_0)]\}, \tag{17}$$

$$\vec{D} = \hat{\epsilon}_2 \vec{E}, \tag{18}$$

where $\hat{L}_2$ and $\hat{\epsilon}_2$ are the elastic stiffness and the permittivity tensor of the particle, respectively. As before, such a constitutive equation can be also written through the generalized variables defined in Eq. (15), by obtaining

$$\Sigma_{iJ} = (\Lambda_2)_{iJMn}(Z_{Mn} - Z_{\mu Mn}) \quad \text{or} \quad \hat{\Sigma} = \hat{\Lambda}_2(\hat{Z} - \hat{Z}_{\mu}), \tag{19}$$

where the tensor $\hat{\Lambda}_2$ represents the elastic and dielectric properties (without piezoelectric effects). Here, $\hat{Z}_{\mu}$ is a generalized strain defined as follows:

$$\hat{Z}_{\mu} = \begin{bmatrix} \hat{\varepsilon}_{\mu}(\vec{\gamma}) - \hat{\varepsilon}_{\mu}(\vec{\gamma}_0) \\ \hline \vec{0} \end{bmatrix}. \tag{20}$$

At this point, we know the constitutive equations of the matrix [see Eq. (16)] and of the inhomogeneity [see Eq. (19)]. The analysis of this configuration can be conducted by applying the piezoelectric Eshelby theory.[46–48] We assume that the whole structure is subjected to an external uniform electric field $\vec{E}^{\infty}$ and an external strain $\hat{\epsilon}^{\infty}$. They are both collected into the generalized remote field $\hat{Z}^{\infty}$,

$$\hat{Z}^{\infty} = \begin{bmatrix} \hat{\varepsilon}^{\infty} \\ \hline -\vec{E}^{\infty} \end{bmatrix}. \tag{21}$$

We are searching for the perturbation to these uniform fields induced by the presence of the inhomogeneity. The equivalence principle, which we are going to illustrate, has been summarized in Fig. 2. The actual presence of an inhomogeneity can be described by the superimposition of the effects generated by two different situations A and B. The first situation is very simple because it considers the effects of the remote fields in an homogeneous matrix without the inhomogeneity. In such a case, we simply observe that the fields remain uniform in the entire space. The situation B corresponds to an inclusion scheme (eigenfield distributed uniformly in the particle) where the eigenfield $\hat{Z}^*$ is still unknown and it can be determined by imposing the equivalence between the original problem and the superimposition A+B. The total fields inside the particle can be obtained summing up the two contributions A and B as follows:

$$\hat{Z} = \hat{Z}^{\infty} + \hat{S}\hat{Z}^*, \quad \hat{\Sigma} = \hat{\Lambda}_1 \hat{Z}^{\infty} + \hat{\Lambda}_1(\hat{S} - \hat{I})\hat{Z}^*, \tag{22}$$

where $\hat{S}$ is the piezoelectric Eshelby tensor defined in Appendix B. It is obtained for describing the response of an inclusion problem: if the inclusion is quantified by a uniform eigenfield $\hat{Z}^*$, then the induced internal field is uniform and

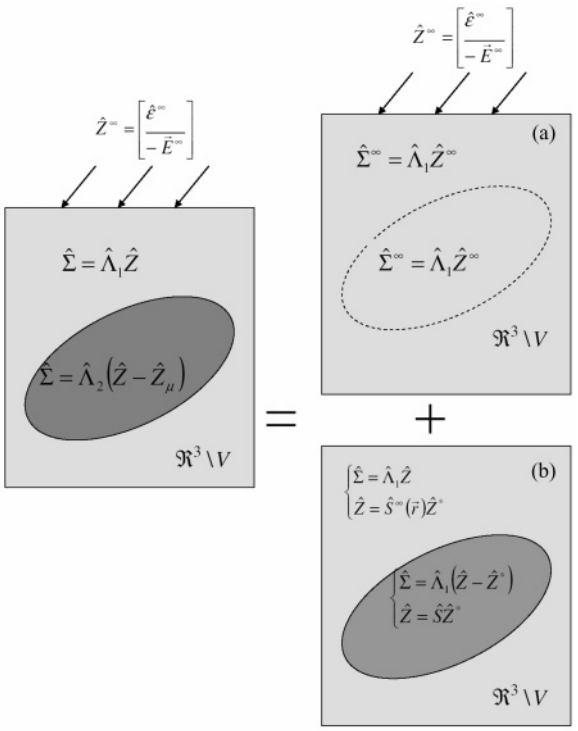

FIG. 2. Scheme describing the Eshelby equivalence principle. The problem A corresponds to a uniform medium $\hat{\Lambda}_1$ with the remotely applied field $\hat{Z}^\infty$. The problem B represents an inclusion problem with eigenfield $\hat{Z}^*$ and without external actions. The superimposition of subproblems A and B allows us to analyze the original scheme of the particle embedded in the matrix.

it is given by $\hat{S}\hat{Z}^*$ ($\hat{S}$ is the so-called internal-points Eshelby tensor), while the external field is given by $\hat{S}^\infty(\vec{r})\hat{Z}^*$ [$\hat{S}^\infty(\vec{r})$ is the so-called external-points Eshelby tensor]. Therefore the Eshelby tensor $\hat{S}$ represents the linear relationship between the eigenfield and the effective field induced inside the particle. Now, the eigenfield $\hat{Z}^*$ can be found imposing the correct behavior of the particle given in Eq. (19). Substituting Eq. (22) in Eq. (19), we obtain the tensor equation for $\hat{Z}^*$:

$$\hat{\Lambda}_1\hat{Z}^\infty + \hat{\Lambda}_1(\hat{S}-\hat{I})\hat{Z}^* = \hat{\Lambda}_2(\hat{Z}^\infty + \hat{S}\hat{Z}^* - \hat{Z}_\mu). \quad (23)$$

Solving Eq. (23), we obtain the equivalent eigenfield

$$\hat{Z}^* = \left[\left(\hat{I}-\hat{\Lambda}_1^{-1}\hat{\Lambda}_2\right)^{-1} - \hat{S}\right]^{-1} \times \left[\hat{Z}^\infty - \left(\hat{I}-\hat{\Lambda}_2^{-1}\hat{\Lambda}_1\right)^{-1}\hat{Z}_\mu\right]. \quad (24)$$

The combination of Eqs. (22) and (24) yields all the electric and elastic fields inside the particle. Of course, this procedure assumes that the technological assembling processes are able to generate a quite perfect particle-matrix interface. In fact, it is well known that the behavior of nanostructured materials is deeply affected by interface features occurring at the boundary between different phases.[49–51] As final result, the local stress depends on the external electric and elastic fields and on the magnetization direction: $\hat{T} = \hat{T}(\hat{\varepsilon}^\infty, \vec{E}^\infty, \vec{\gamma})$. In fact, by means of Eqs. (22) and (24), we can extract the elastic stress and we can write an explicit relation given by

$$\hat{T} = \hat{C}\hat{\varepsilon}^\infty + \hat{D}\vec{E}^\infty + \hat{F}[\hat{\varepsilon}_\mu(\vec{\gamma}) - \hat{\varepsilon}_\mu(\vec{\gamma}_0)]. \quad (25)$$

It represents the main result of the present section. Here, the tensors $\hat{C}$, $\hat{D}$, and $\hat{F}$ can be easily identified through Eqs. (22) and (24) and the definitions given in Eq. (15). A different but equivalent technique for obtaining such tensors is described in Appendix C. This alternative procedure is based on the uncoupled electric $\hat{S}_e$ and elastic $\hat{S}_\varepsilon$ Eshelby tensors. It is useful for avoiding the calculation of the piezoelectric Eshelby tensor $\hat{S}$ introduced in Appendix B; this point is important both for the conceptual point of view and for the numerical implementation.

V. STATIC BEHAVIOR OF THE SYSTEM

Summing up, the set of equations describing the memory system is constituted of the energy minimization [see Eq. (1)], the coupling with the external magnetic field $\vec{H} = \vec{H}(\vec{H}^\infty, \vec{\gamma})$ [see Eq. (9)] and the coupling with the external electric and elastic fields $\hat{T} = \hat{T}(\hat{\varepsilon}^\infty, \vec{E}^\infty, \vec{\gamma})$ [see Eq. (25)]. The first minimization problem is constrained by the condition $\vec{\gamma}\cdot\vec{\gamma} = 1$ ($\vec{\gamma}$ is a unit vector). So, we can apply the Lagrange method, which converts the constrained problem into an unconstrained minimization of the function $\mathcal{L}(\vec{\gamma},\lambda) = w(\vec{\gamma}) - \lambda(\vec{\gamma}\cdot\vec{\gamma} - 1)$, where λ is the so-called Lagrange multiplier. Therefore we consider the equations $\partial\mathcal{L}/\partial\gamma_i = 0$ (for $i = 1,2,3$) and $\partial\mathcal{L}/\partial\lambda = 0$. We straightforwardly obtain the complete system:

$$\begin{cases} 2\lambda\gamma_i = -\mu_0 M_s H_i + \frac{\partial\varphi_a(\vec{\gamma})}{\partial\gamma_i} - \hat{T} : \frac{\partial\hat{\varepsilon}_\mu(\vec{\gamma})}{\partial\gamma_i} \\ \vec{\gamma}\cdot\vec{\gamma} = 1 \\ \vec{H} = \hat{A}\vec{H}^\infty + \hat{N}\vec{\gamma} \\ \hat{T} = \hat{C}\hat{\varepsilon}^\infty + \hat{D}\vec{E}^\infty + \hat{F}[\hat{\varepsilon}_\mu(\vec{\gamma}) - \hat{\varepsilon}_\mu(\vec{\gamma}_0)] \end{cases}. \quad (26)$$

We can now substitute the last two relations in the first one, eventually obtaining

$$2\lambda\gamma_i = -\mu_0 M_s(\hat{A}\vec{H}^\infty + \hat{N}\vec{\gamma})_i + \frac{\partial\varphi_a(\vec{\gamma})}{\partial\gamma_i} - \{\hat{C}\hat{\varepsilon}^\infty + \hat{D}\vec{E}^\infty + \hat{F}[\hat{\varepsilon}_\mu(\vec{\gamma}) - \hat{\varepsilon}_\mu(\vec{\gamma}_0)]\} : \frac{\partial\hat{\varepsilon}_\mu(\vec{\gamma})}{\partial\gamma_i}. \quad (27)$$

By exploiting the symmetries of tensors $\hat{N}$ and $\hat{F}$ (introduced in Sec. III and Appendix C, respectively) we can simply rewrite Eq. (27) as follows:

$$2\lambda\gamma_i = -\mu_0 M_s \frac{\partial}{\partial\gamma_i}(\vec{\gamma}\cdot\hat{A}\vec{H}^\infty) - \frac{1}{2}\mu_0 M_s \frac{\partial}{\partial\gamma_i}(\vec{\gamma}\cdot\hat{N}\vec{\gamma}) + \frac{\partial\varphi_a(\vec{\gamma})}{\partial\gamma_i} - \frac{\partial}{\partial\gamma_i}[\hat{C}\hat{\varepsilon}^\infty : \hat{\varepsilon}_\mu(\vec{\gamma})] - \frac{\partial}{\partial\gamma_i}[\hat{D}\vec{E}^\infty : \hat{\varepsilon}_\mu(\vec{\gamma})] - \frac{1}{2}\frac{\partial}{\partial\gamma_i}[\hat{F}\hat{\varepsilon}_\mu(\vec{\gamma}) : \hat{\varepsilon}_\mu(\vec{\gamma})] + \frac{\partial}{\partial\gamma_i}[\hat{F}\hat{\varepsilon}_\mu(\vec{\gamma}_0) : \hat{\varepsilon}_\mu(\vec{\gamma})]. \quad (28)$$

The previous expression combined with the condition $\vec{\gamma}\cdot\vec{\gamma} = 1$ corresponds to a constrained minimization of a new energy function defined as

$$\tilde{w} = -\mu_0 M_s\vec{\gamma}\cdot\hat{A}\vec{H}^\infty - \tfrac{1}{2}\mu_0 M_s\vec{\gamma}\cdot\hat{N}\vec{\gamma} + \varphi_a(\vec{\gamma}) - \hat{C}\hat{\varepsilon}^\infty : \hat{\varepsilon}_\mu(\vec{\gamma}) - \hat{D}\vec{E}^\infty : \hat{\varepsilon}_\mu(\vec{\gamma}) - \tfrac{1}{2}\hat{F}\hat{\varepsilon}_\mu(\vec{\gamma}) : \hat{\varepsilon}_\mu(\vec{\gamma}) + \hat{F}\hat{\varepsilon}_\mu(\vec{\gamma}_0) : \hat{\varepsilon}_\mu(\vec{\gamma}). \quad (29)$$

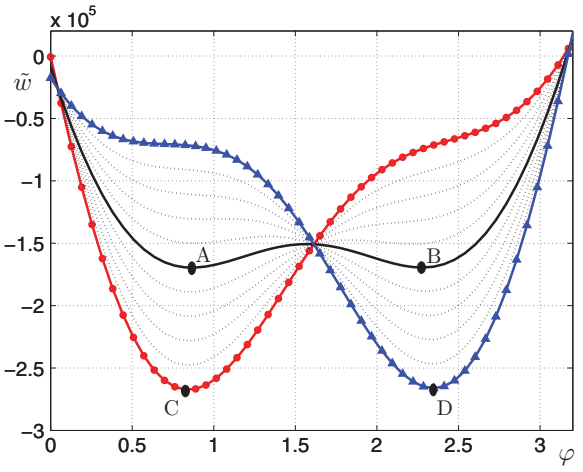

FIG. 3. (Color online) Curves $\tilde{w}(\varphi)$ [J/m^3] for different values of the applied voltage. The blue line (with triangles) corresponds to -0.5 V or $+3.85 \times 10^6$ V/m (traction), while the red line (with circles) corresponds to $+0.5$ V or -3.85×10^6 V/m (compression). The angle φ in the range $(0,\pi)$ is measured in radians. The solid black line corresponds to 0 V and shows the couple of stable points A and B.

This relation is very convenient since it leads directly to the final magnetization orientation in terms of the external fields applied to the structure (in other terms, $\tilde{w}$ represents the thermodynamic potential at given $\vec{H}^\infty$, $\hat{\varepsilon}^\infty$, and $\vec{E}^\infty$, whereas w represents the potential at given $\vec{H}$ and $\hat{T}$). A complete software procedure has been implemented in order to evaluate Eq. (29), where the involved tensors are calculated through the schemes outlined in Appendixes B and C.

The general procedure here proposed is valid for any external fields $\vec{H}^\infty$, $\hat{\varepsilon}^\infty$, and $\vec{E}^\infty$, applied to the structure. In the following, we suppose that there is no direct mechanical action on the system and, therefore, we set $\hat{\varepsilon}^\infty = 0$ everywhere. We also adopt an external magnetic field $\vec{H}^\infty$ along the y axis (see Fig. 1): the competition of the latter with the uniaxial anisotropy of the magnetoelastic particle (along the x axis) generates two stable positions for $\vec{M}$ corresponding to the possible states of the memory element: "0" and "1" (blue and red arrows in Fig. 1). These two positions appear around $\varphi = \pi/4$ and $\varphi = 3\pi/4$ if $H^\infty = 50 \times 10^4$A/m as can be simply proved by minimizing Eq. (29) with $\vec{E}^\infty = 0$. In Fig. 3, one can find the plot of the energy function $\tilde{w}$ [see Eq. (29)] with $\vec{\gamma} = (\cos\varphi, \sin\varphi, 0)$ (on the plane $z = 0$) in terms of the angle φ. The solid black line corresponds to the case with $\vec{E}^\infty = 0$ and the bistable behavior is identified by the couple of minima A and B.

The external electric field $\vec{E}^\infty$ (here applied along the direction at $\varphi = 3\pi/4$) and the piezoelectric matrix represent the system used for switching the state of the memory. We assume that the matrix is constituted of lead zirconate titanate (PZT-5H) and it is polarized along the direction identified by $\varphi = 3\pi/4$. The tensor $\hat{\Lambda}_1$ takes properly into account the anisotropic character of the matrix and it has been obtained by rotating the properties, which can be found in the documentation of the PZT-5H piezoelectric matrix. The geometry of the system implies that the structure is mechanically stressed along the direction at $\varphi = 3\pi/4$ when a voltage is applied on the electrodes. This configuration allows compressive or tensile stress, depending on the sign of the voltage. In Fig. 3, one can also find the plot of the energy function $\tilde{w}$ for different values of the applied voltage: it ranges from 0.5 V (red line with circles) to -0.5 V (blue line with triangles) corresponding to an electric field E^∞ ranging in $(-3.85, +3.85)\times10^6$ V/m (for a distance between the electrodes $d = 130$ nm). In Fig. 4, we have also reported the polar plot of the energy profile, obtained through the parametric representation $([\tilde{w}(\varphi) + \delta]\cos\varphi, [\tilde{w}(\varphi) + \delta]\sin\varphi)$. The value of the parameter δ has been fixed for obtaining a positive radius $\tilde{w}(\varphi) + \delta > 0$ for any angle φ.

It is evident by the profile of the energy function (see Figs. 3 and 4) that the applied electric field is able to switch the state of the memory without the knowledge of the stored bit (nontoggle property): if we start from the point B, the application of the voltage $V = 0.5$ V (compression) drives the system to the point C; after the removal of the voltage the system remains in the state A. The inverse path starts from point A and after the application of the voltage $V = -0.5$ V (traction) arrives at point D; as before, the removal of the potential leaves the system in the point B.

It is also important to investigate the fine variations of the angle φ of the magnetization direction in correspondence of the stable points with different applied fields. In Fig. 5, the angular positions of the points C and D are reported versus E^∞ and H^∞. We remark that when $E^\infty = 0$ we have $\varphi(C) = \varphi(A)$ and $\varphi(D) = \varphi(B)$. We observe that $\varphi(C)$ and $\varphi(D)$ vary moderately with E^∞ also with a fixed magnetic field H^∞. In this work, as mentioned above, we use the fixed value $H^\infty = 50 \times 10^4$A/m, which implies two quite orthogonal stable positions around $\pi/4$ and $3\pi/4$.

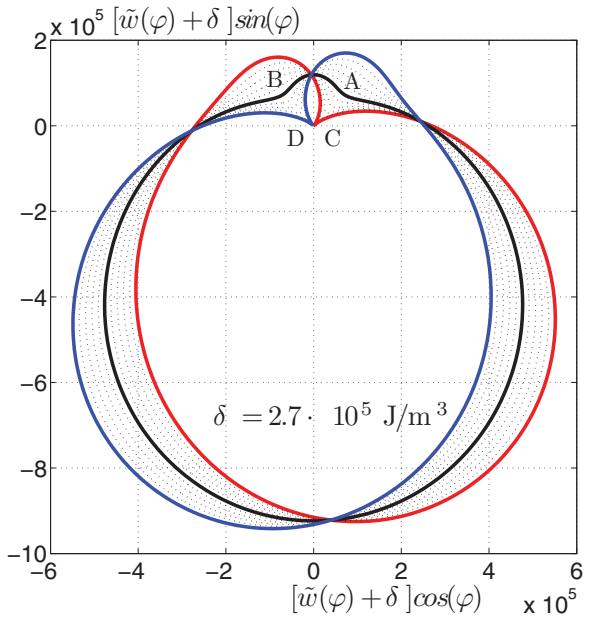

FIG. 4. (Color online) Polar plot of the energy profile $\tilde{w}(\varphi)$ (J/m^3). It corresponds to the parametric representation $([\tilde{w}(\varphi) + \delta]\cos\varphi, [\tilde{w}(\varphi) + \delta]\sin\varphi)$ where $\delta = 2.7 \times 10^5$J/m^3 has been added for obtaining $\tilde{w}(\varphi) + \delta > 0$ everywhere. The red, blue, and black lines have the same meaning of Fig. 3.

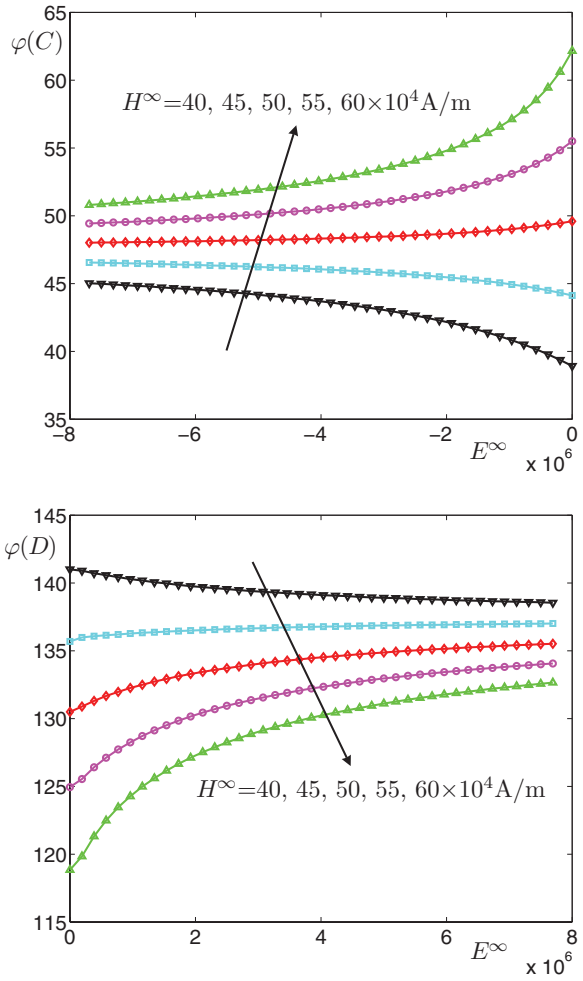

FIG. 5. (Color online) Fine variations of the angular positions $\varphi(C)$ and $\varphi(D)$ (in degrees) where C and D are the two stable points defined in Figs. 3 and 4. They are represented vs the externally applied fields E^∞ and H^∞. We observe that when $E^\infty = 0$, we have $\varphi(C) = \varphi(A)$ and $\varphi(D) = \varphi(B)$.

This analysis describes the static behavior of the system and the commutation strategy mediated by the piezoelectric matrix. We must now validate these results in the dynamic regime.

VI. DYNAMIC BEHAVIOR OF THE SYSTEM

Given the size of the magnetic particle and the value of the exchange stiffness constant ($A = 10^{-11}$ J/m for terfenol),[52,53] the magnetic system is assumed to be monodomain and all the spins behave collectively. Therefore the dynamics of the magnetization direction $\vec{\gamma}$ is described by the LLG equation[11,12]

$$\frac{d\vec{\gamma}}{dt} = -\frac{\mathcal{G}}{M_s(1+\alpha^2)}\left[\vec{\gamma}\wedge\frac{\partial\tilde{w}}{\partial\vec{\gamma}} - \alpha\vec{\gamma}\wedge\left(\vec{\gamma}\wedge\frac{\partial\tilde{w}}{\partial\vec{\gamma}}\right)\right], \quad (30)$$

where $\mathcal{G}$ is the gyromagnetic ratio, α is the Gilbert damping parameter and $\frac{\partial\tilde{w}}{\partial\vec{\gamma}}$ represents the effective field applied to the magnetic dipole. We assumed $\alpha = 0.3$, which is a reasonable value for ferrimagnetic rare earth-transition metal (RE-TM) alloys,[54] and $\mathcal{G} = g\mu_B/\hbar = 1.76\times10^{11}$ rad s^{-1}T^{-1} ($g = 2$ is the Landé factor and μ_B is the Bohr magneton). While the procedure developed in previous sections for obtaining $\tilde{w}$ is exact at stationary regime, the use of $\tilde{w}$ in the LLG Eq. (30) is an approximation, which must be justified as follows. The system comprised between the two electrodes can be considered as a capacitor, which capacitance is $C = \epsilon_1 S/d$, where $\epsilon_1 = 3000\epsilon_0$ is the dielectric constant of PZT and S the total area. With a load resistance $R = 10\ \Omega$, the resulting time constant is $\tau = RC \approx 3fs$. Therefore we have $\tau \ll 1/(\mu_0\mathcal{G}H_{\max})$, where $H_{\max}$ is the highest value of the effective magnetic field: it means that we can consider instantaneous electric field and mechanical stress applied to the structure during the transitional phases. To further justify the use of $\tilde{w}$ in Eq. (30), we also remark that $t_m \gg t_0 = 1/f_0$ where $t_m \simeq 0.4\times10^{-9}$ s is the magnetic switching time (see below for details) and $f_0 \simeq 10^{12}$ s^{-1} is the elastic eigenfrequency of the particle.

In Fig. 6, the results of the integration of Eq. (30) are shown for two different values of the applied voltage: ±0.3 V (which means $E^\infty = \pm2.3\times10^6$ V/m) and ±0.5 V (which means $E^\infty = \pm3.85\times10^6$ V/m). A complete cycle with the two switching phases is represented and reveals two important properties: (i) the transition times are always in the subnanosecond scale (<0.4 ns) and (ii) such times decrease with larger applied voltages (in a given range, see below). While in the static analysis of the system we have described the commutation strategy on the plane, in the actual dynamic case, the complex behavior is the result of the interplay between the in-plane and the out-of-plane motion of $\vec{\gamma}(t)$. This point becomes evident by the observation of the component γ_z in the second panel of Fig. 6 (see also Fig. 8 below).

In Fig. 6, we can also find the behavior of the local stress during the complete cycle. We have defined the quantities $T_{\vec{n}} = \vec{n}\cdot\hat{T}\vec{n}$ and $T_{\vec{m}} = \vec{m}\cdot\hat{T}\vec{m}$ where $\vec{n} = (\sqrt{2}/2,\sqrt{2}/2,0)$ and $\vec{m} = (-\sqrt{2}/2,\sqrt{2}/2,0)$. They represent the specific force (N/m^2) along the directions at $\varphi = \pi/4$ and $\varphi = 3\pi/4$, respectively. We remark that when these quantities are positive we have a traction and when they are negative a compression. In the phase D (writing of the bit "1"), we find a traction along $\vec{m}$ ($T_{\vec{m}} \simeq 90$ MPa with -0.5 V and $T_{\vec{m}} \simeq 55$ MPa with -0.3 V) induced by the positive electric field applied to the piezoelectric matrix. Conversely, in the phase C (writing of the bit "0") a compression along $\vec{m}$ ($T_{\vec{m}} \simeq -60$ MPa with $+0.5$ V and $T_{\vec{m}} \simeq -20$ MPa with $+0.3$ V) is generated by the negative electric field. It is important to observe that the stable points A and B are characterized by a nonzero state of stress since the tractions or compressions are absent only when the magnetization is oriented along the x axis (in both directions). Therefore the state of stress in A and B is maintained at the levels indicated in Fig. 6 by the magnetic field $\vec{H}^\infty$. Interestingly enough, we observe that the values of $T_{\vec{n}}$ and $T_{\vec{m}}$ are inverted passing from the point A to the point B because of the symmetry of the system. Nevertheless, such a geometrical symmetry does not lead to the same dynamical features of the switching phases B-C and A-D. In fact, the phase B-C is characterized by a compression inducing a *planar anisotropy* from the magnetic point of view (on the plane perpendicular to $\vec{m}$). On the other hand, the phase A-D is characterized by a traction inducing an *axial anisotropy* for the magnetization (along the direction $\vec{m}$).

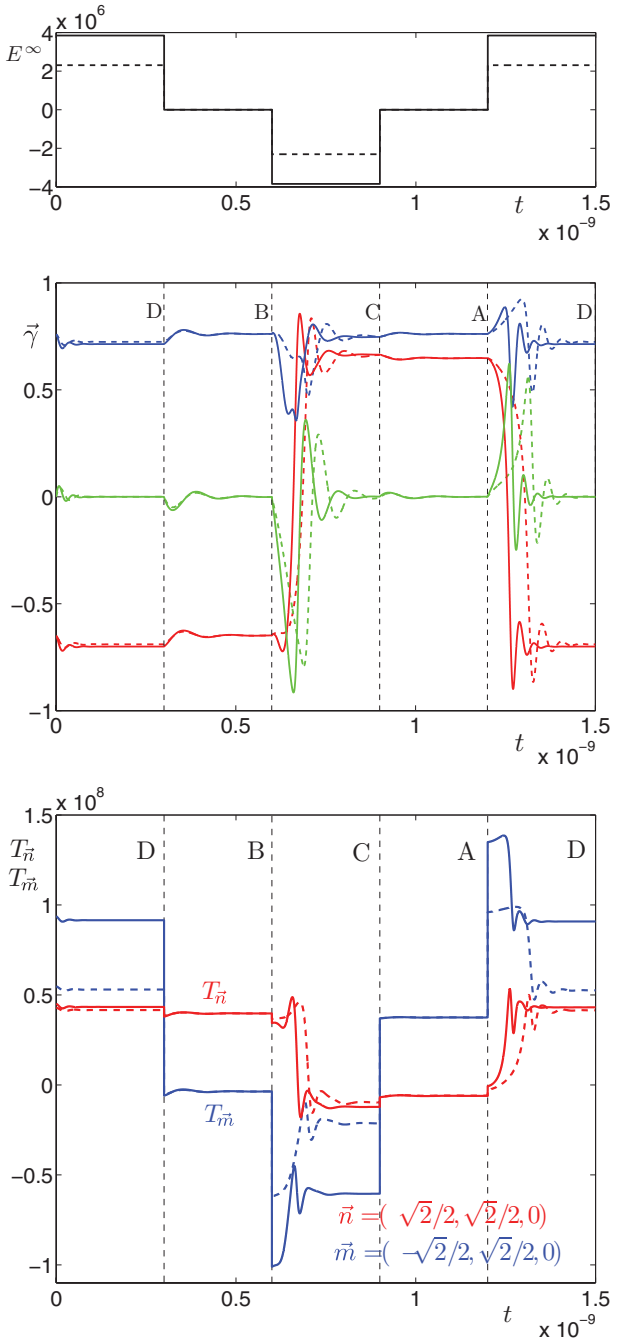

FIG. 6. (Color online) Time behavior of the imposed electric field E^{∞} (V/m) (first panel) and the corresponding evolution of the magnetization direction $\vec{\gamma}$ (γ_x red, γ_y blue and γ_z green in the second panel) for a voltage equals to ± 0.5 V (solid lines) and ± 0.3 V (dashed lines). In the third panel we have represented the dynamic behavior of the local stress (N/m^2). The tractions $T_{\vec{n}} = \vec{n} \cdot \hat{T}\vec{n}$ and $T_{\vec{m}} = \vec{m} \cdot \hat{T}\vec{m}$ along the directions $\vec{n} = (\sqrt{2}/2, \sqrt{2}/2, 0)$ and $\vec{m} = (-\sqrt{2}/2, \sqrt{2}/2, 0)$ are shown.

In particular, the differences between the physical phenomena involved in phases B-C and A-D are reflected in the switching times as reported in Fig. 7. We consider the magnetization direction $\vec{\gamma} = (\gamma_x, \gamma_y, \gamma_z)$ and the scalar quantity $G = |\gamma_x| + |\gamma_y| + |\gamma_z|$ as functions of the time during the commutation phases. We define the the switching time as the

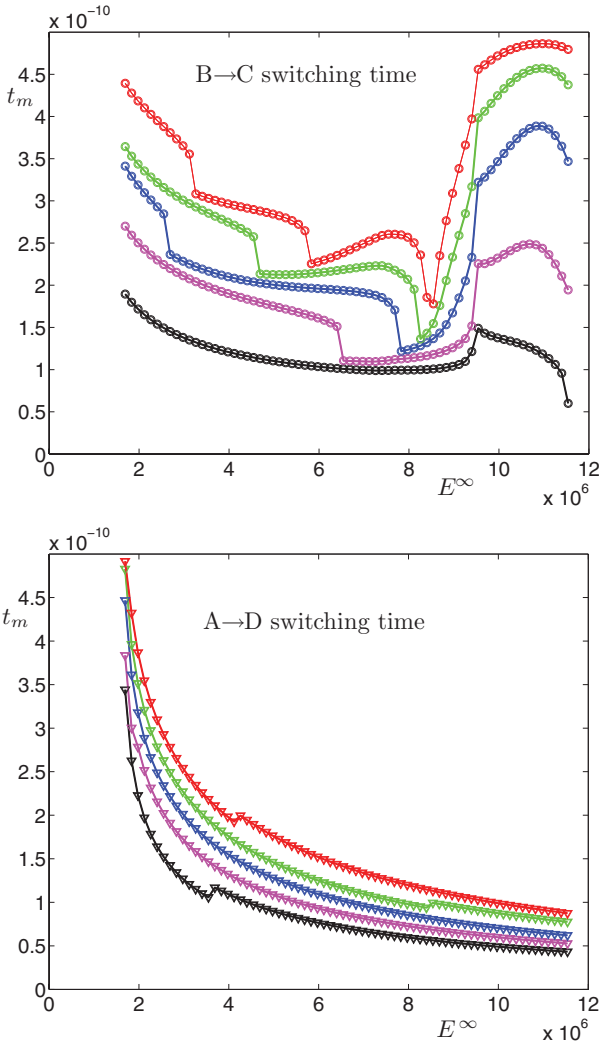

FIG. 7. (Color online) Switching times of the commutation phases B-C (top panel) and A-D (bottom panel) as function of the applied electric field E^{∞} in the range 1.7×10^6–11.5×10^6 V/m (corresponding to the electric potential between 0.22 and 1.5 V). The different curves (from the top to the bottom) correspond to the values $\varrho = 1/1000, 1/300, 1/100, 1/30$, and $1/10$ of the precision parameter.

first instant of time t_m (of the commutation phase) satisfying the condition $|G(t) - G(\infty)| < \varrho$ for any $t > t_m$. Here, the parameter ϱ represents the precision requested, which, of course, modifies the resulting switching time. In Fig. 7, we have used the values $\varrho = 1/1000, 1/300, 1/100, 1/30$, and $1/10$ and they correspond to the curves from the top to the bottom for both panels. While the switching time of the phase A-D is a monotonically decreasing function of the applied electric field, the switching time of the phase B-C reveals a more complex scenario. In particular, we observe that in correspondence to the electric field $E^{\infty} = 9.5 \times 10^6$ V/m there is a transition where the B-C switching time increases considerably. Therefore the region where $E^{\infty} > 9.5 \times 10^6$ V/m is not convenient for the memory element. We conclude that the optimal working region (from the switching time point of view) is defined by an electric potential ranging from 0.25 to 1 V. In fact, in this interval, we have $t_m < 0.4$ ns with the better precision defined by $\varrho = 1/1000$.

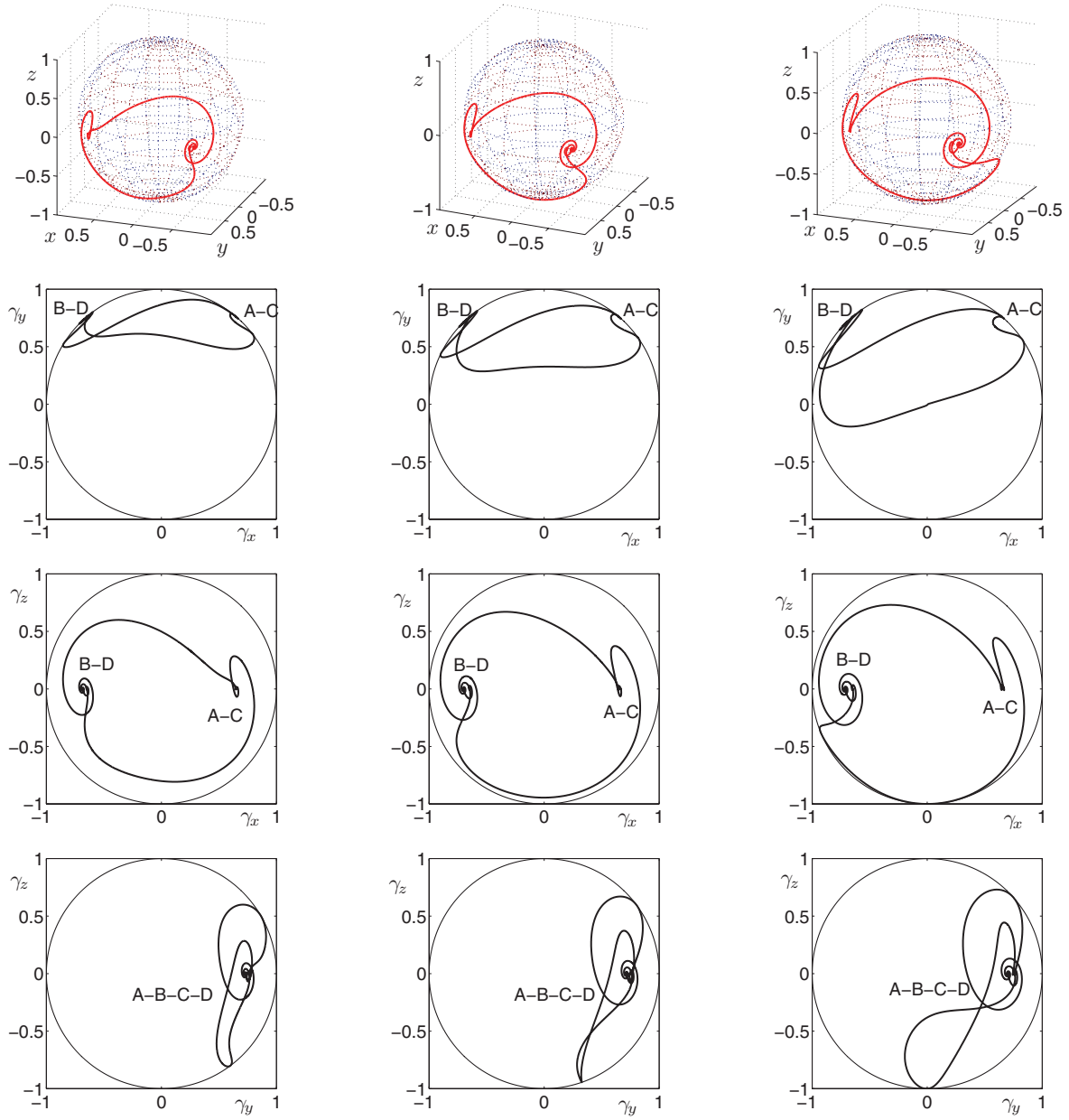

FIG. 8. (Color online) Time behavior of the magnetization direction $\vec{\gamma}$ for a voltage equals to ± 0.25 (first column), ± 0.5 (second column), and ± 1 V (third column).

In order to better understand the differences between the switching phases B-C and A-D we have also shown in Fig. 8 the trajectories of the magnetization direction $\vec{\gamma}$ for three different values of the electric field (± 0.25, ± 0.5, and ± 1 V). Both the three-dimensional view and the orthogonal projections reported in Fig. 8 demonstrate that the trajectories B-C and A-D are not reversible: it means that each commutation phase follows its own independent path. Moreover, we can better explain the switching time transition observed for $E^{\infty} = 9.5 \times 10^6$ V/m: we focus our attention to the projection on the plane (γ_z, γ_x) in Fig. 8. The upper curve represents the A-D commutation phase (going to the left), while the lower one corresponds to the B-C transition (going to the right). It is evident that the A-D trajectory is always regular for any value of the applied electric field while the B-C trajectory exhibits a *singular* reversal point after the start from the point B, which is more and more pronounced with an increasing electric field. Further, for electric fields $E^{\infty} > 9.5 \times 10^6$V/m the topology of the trajectory is strongly modified by the reversal point and the switching time increases significantly.

To conclude, we discuss the results of the energetic analysis of the system. The dissipated energy during switching processes derives from the charge/discharge of the effective capacitor and from the damped precession of the magnetization:[32] the total energy amount for a switching phase corresponds to $3 \times 10^{-17} J$ with the applied voltage of ± 0.3 V and to $8 \times 10^{-17} J$ with ± 0.5 V. These values are strongly competitive when compared with most nonvolatile memory technologies.[55] In fact, some values of the switching energy are as follows: $0.02 pJ$ for the spin transfer torque RAM

(STTRAM), $2pJ$ for the ferroelectric RAM (FRAM), $2pJ$ for the copper bridge RAM (CBRAM), $2pJ$ for the dynamic RAM (DRAM), and $10pJ$ for the carbon nanotube RAM (NRAM). A complete table for drawing other comparisons can be found elsewhere.[55] Moreover, the thermal stability can be assured by the energy barrier between the states A and B corresponding to $1.7 \times 10^{-18} J \simeq 400 k_B T$. This value of the energy barrier is sufficiently high to inhibit spontaneous magnetization flipping due to thermal effects. We admit, however, that for quantifying the possible perturbation induced by the temperature we should use the stochastic LLG equation or the corresponding Fokker-Planck equation.[56,57] This analysis is beyond the scope of the present paper. We finally remark that the energy barrier can be potentially varied by changing the external magnetic field and the strength of the anisotropy (by maintaining the orthogonality of the states). This point can be exploited in magnetologic applications where a low and variable energy barrier is requested.[58]

VII. CONCLUSIONS

In this work, we have developed a complete procedure for modeling the behavior of a particle/matrix multiferroic heterostructure and we have presented its application to a new paradigmatic memory element composed of a ferromagnetic nanoparticle embedded in a piezoelectric matrix. For the sake of definiteness, we have assumed a terfenol ($TbFe_2$) particle in a PZT-5H matrix. Nevertheless, this analysis can be exploited for studying several different heterogeneous systems with similar geometrical structures.

The whole analysis has been conducted in two different steps: at first, the determination of the actual fields within the particle has been approached through the multiphysics Eshelby theory. The ellipsoidal shape and the nanosize of the ferromagnetic element assure the uniformity of the internal fields and induce the monodomain behavior, which is essential for obtaining well defined and recognizable magnetization states. The Eshelby theory allows us to determine the exact relation between the externally applied fields and those induced in the embedded particle. In particular, we have proved the possibility to obtain two orthogonal states generated by the competition between the magnetic anisotropy with the Zeeman energy term. Then, we have developed a commutation scheme with the help of the coupling with the piezoelectric matrix.

As second step, the analysis is completed by considering the LLG equation, describing the dynamics of the magnetization during the switching cycle. Its application reveals a complex scenario generated by the interplay between the in-plane and the out-of-plane motion of magnetization vector. In particular, we have proved that the switching time is not a monotonic function of electric field applied during the commutation phases. This can be explained by observing that high values of the electric field may cause ripples and unexpected reversal points, which may prolong or stop the switching processes. Moreover, we have not observed the reversibility and the symmetry of the two trajectories (in the opposite directions) between the states. Anyway, we have numerically proved that there exists a range of values for the electric field, which assures the correct operation of the device. We have then performed the energetic analysis of the system.

To conclude, the thorough combination of the nanomechanical techniques (i.e., the Eshelby formalism) with the spin dynamics methods (grounded on the Landau-Lifshitz-Gilbert equation) represents a multidisciplinary exemplary approach properly suited to fully characterize the coupled response of several heterostructures and it can be used to design the corresponding devices with specific desired properties.

ACKNOWLEDGMENTS

Y. Dusch was funded by the Direction Générale de l'Armement (DGA-France). This work is supported by the Agence Nationale de la Recherche ANR (France) through the PNano NAMAMIS project and by the Russian Federation Ministry of Education and Sciences (project N. 2011-1.9-519-021-141). S. Giordano acknowledges financial support by "Fondation Centrale Initiatives" under project "Continuum approach for studying the static and dynamic behavior of piezo-magneto-elastic composite materials". The authors would like to thank Alain Cappy for fruitful discussions.

APPENDIX A: ENERGIES, COUPLINGS, AND SYMMETRIES

By considering Maxwell equation for the matter, it is possible to prove that the time variation of the energy density u associated with the electric field is given by[43,59]

$$\frac{du}{dt} = E_i \frac{dD_i}{dt}. \tag{A1}$$

Now, if we suppose that the energy density directly depends on the displacement vector $u = u(\vec{D})$, we simply obtain $\frac{du}{dt} = \frac{\partial u}{\partial D_i}\frac{dD_i}{dt} = E_i \frac{dD_i}{dt}$ and therefore any constitutive equation for the electric behavior of a material can be derived by the energy function by means of the relation

$$E_i = \frac{\partial u(\vec{D})}{\partial D_i}. \tag{A2}$$

In this context, we have considered the complete uncoupling between the electric and the elastic properties.

On the other hand, it is possible to verify the following relation giving the rate of change of the elastic energy density u during a time-dependent deformation,[60]

$$\frac{du}{dt} = T_{ij} \frac{d\epsilon_{ij}}{dt}. \tag{A3}$$

If we suppose that the strain energy function u depends only on the state of strain of the system $u = u(\epsilon_{ij})$, then we can write $\frac{du}{dt} = \frac{\partial u}{\partial \epsilon_{ij}}\frac{d\epsilon_{ij}}{dt} = T_{ij}\frac{d\epsilon_{ij}}{dt}$, and therefore any constitutive equation of an elastic material can be derived by the strain energy function by means of the relation

$$T_{ij} = \frac{\partial u(\hat{\epsilon})}{\partial \epsilon_{ij}}. \tag{A4}$$

This result holds on for the uncoupled elastic case.

In order to take into account all the possible couplings among the electric and the elastic quantities, we generalize Eqs. (A1) and (A3) with the following relation giving the time

variation of the total energy,

$$\frac{du}{dt} = T_{ij}\frac{d\epsilon_{ij}}{dt} + E_i\frac{dD_i}{dt}, \tag{A5}$$

where we have supposed an arbitrarily nonlinear energy function (density) $u = u(\hat{\epsilon}, \vec{D})$. Following the same approach used within the uncoupled cases, we obtain the constitutive equations in terms of the energy function:

$$T_{ij} = \frac{\partial u(\hat{\epsilon}, \vec{D})}{\partial \epsilon_{ij}}, \quad E_i = \frac{\partial u(\hat{\epsilon}, \vec{D})}{\partial D_i}. \tag{A6}$$

We may introduce the following generalized quantities:

$$\hat{\Sigma}_0 = [\hat{T}\,|\,\vec{E}] \quad \text{and} \quad \hat{Z}_0 = \begin{bmatrix} \hat{\varepsilon} \\ \vec{D} \end{bmatrix} \tag{A7}$$

that allow for a compact notation of the previous energy balances Eqs. (A5) and (A6):

$$\frac{du}{dt} = \Sigma_{0,iJ}\frac{dZ_{0,Ji}}{dt} \quad \text{and} \quad \Sigma_{0,iJ} = \frac{\partial u}{\partial Z_{0,Ji}}. \tag{A8}$$

We observe that $\hat{\Sigma}_0$ is represented (once fixed a reference frame) by a matrix 3×4, while $\hat{Z}_0$ by a matrix 4×3. Therefore we use capital letters for indexes ranging in 1, 2, 3 and small letters for indexes ranging in 1, 2, 3, 4. In the case of a linear system, we can introduce a linear relationship between $\hat{\Sigma}_0$ and $\hat{Z}_0$:

$$\Sigma_{0,iJ} = \Lambda_{0,iJKh}Z_{0,Kh} \quad \text{or} \quad \hat{\Sigma}_0 = \hat{\Lambda}_0\hat{Z}_0. \tag{A9}$$

Since $\Lambda_{0,iJKh} = \partial\Sigma_{0,iJ}/\partial Z_{0,Kh}$ and, at the same time, $\Sigma_{0,iJ} = \partial u/\partial Z_{0,Ji}$, we obtain the expression $\Lambda_{0,iJKh} = \partial^2 u/\partial Z_{0,Ji}\partial Z_{0,Kh}$, which means that the following symmetry rule holds on: $\Lambda_{0,iJKh} = \Lambda_{0,hKJi}$. By using this symmetry, we can easily obtain the complete expression for the energy function of a piezoelectric system in the form $u = (1/2)\Lambda_{0,iJKh}Z_{0,Ji}Z_{0,Kh}$.

In addition to $\hat{\Sigma}_0$ and $\hat{Z}_0$, it is also possible to use the alternative generalized variables defined in Eq. (15), which are useful to obtain a more convenient formalism for the following developments. We can prove that if $\hat{\Sigma}_0 = \hat{\Lambda}_0\hat{Z}_0$ then $\hat{\Sigma} = \hat{\Lambda}\hat{Z}$ with a tensor $\hat{\Lambda}$ having the same symmetries of the tensor $\hat{\Lambda}_0$. To prove this point, we rewrite Eq. (A9) defining the tensor $\hat{\Lambda}_0$ in explicit form:

$$\hat{T} = \hat{l}\hat{\varepsilon} + \hat{q}\vec{D}, \tag{A10}$$

$$\vec{E} = \hat{q}^T\hat{\varepsilon} + \hat{e}\vec{D}, \tag{A11}$$

with $\hat{l} = \hat{l}^T$ and $\hat{e} = \hat{e}^T$. By algebraic manipulations we obtain

$$\hat{T} = (\hat{l} - \hat{q}\hat{e}^{-1}\hat{q}^T)\hat{\varepsilon} - \hat{q}\hat{e}^{-1}(-\vec{E}), \tag{A12}$$

$$\vec{D} = -\hat{e}^{-1}\hat{q}^T\hat{\varepsilon} - \hat{e}^{-1}(-\vec{E}), \tag{A13}$$

which are the equations defining the tensor $\hat{\Lambda}$; therefore the tensor $\hat{\Lambda}$ has the same symmetries of $\hat{\Lambda}_0$ since $(\hat{l} - \hat{q}\hat{e}^{-1}\hat{q}^T)^T = \hat{l} - \hat{q}\hat{e}^{-1}\hat{q}^T$ and $(-\hat{q}\hat{e}^{-1})^T = -\hat{e}^{-1}\hat{q}^T$. Comparing this result with Eqs. (13) and (14), we can also obtain the equalities $\hat{L}_1 = \hat{l} - \hat{q}\hat{e}^{-1}\hat{q}^T$, $\hat{\epsilon}_1 = \hat{e}^{-1}$, $\hat{Q}_1 = \hat{q}\hat{e}^{-1}$, and $\hat{R}_1 = -\hat{e}^{-1}\hat{q}^T$ (and therefore $\hat{R}_1 = -\hat{Q}_1^T$ as expected).

APPENDIX B: THE PIEZOELECTRIC ESHELBY TENSOR

We take into consideration a stationary regime. From the electric point of view, using the Faraday's law $\vec{\nabla} \times \vec{E} = -\partial\vec{B}/\partial t$ and the condition $\partial\vec{B}/\partial t = 0$, we derive the existence of the electric potential ϕ such that $\vec{E} = -\vec{\nabla}\phi$. Moreover, we assume that $\rho = 0$ (absence of charge density) everywhere in the space and therefore the Gauss's law becomes $\vec{\nabla} \cdot \vec{D} = 0$. From the elastic point of view, we assume that the body forces are absent and, therefore, the stationary condition yields $\partial T_{ji}/\partial x_i = 0$. Thus the main equation under these hypotheses is

$$\frac{\partial\Sigma_{iJ}}{\partial x_i} = 0. \tag{B1}$$

Now, we define as *inclusion* a region of the space where there is an *eigenfield* $Z^*_{Mn}(\vec{x})$ defined through the following constitutive equation:[61]

$$\Sigma_{iJ} = \Lambda_{iJMn}(Z_{Mn} - Z^*_{Mn}). \tag{B2}$$

We assume that $Z^*_{Mn}(\vec{x})$ is given and it is different from zero only in a defined limited region of the space. We also define a generalized potential as $U_M = u_m$ for $M = m \leqslant 3$ (elastic displacement) and $U_M = \phi$ for $M = 4$ (electric potential). Substituting Eq. (B2) in Eq. (B1) and using the definition of the generalized potential, we have

$$\Lambda_{iJMn}\frac{\partial^2 U_M(\vec{x})}{\partial x_i\partial x_n} + b^*_J(\vec{x}) = 0, \tag{B3}$$

where the quantity $b^*_J(\vec{x}) = -\Lambda_{iJMn}\frac{\partial Z^*_{Mn}(\vec{x})}{\partial x_i}$ assumes the role of an effective density of sources equivalent to the eigenfield. We can associate Eq. (B3) with the definition of the Green function in the ordinary way, i.e., by imposing a Dirac source $b^*_J(\vec{x}) = \delta_{AJ}\delta(\vec{x})$ and a fundamental solution $U_M(\vec{x}) = G_{MA}(\vec{x})$. The differential equation defining the Green function is therefore given by

$$\Lambda_{iJMn}\frac{\partial^2 G_{MA}(\vec{x})}{\partial x_i\partial x_n} + \delta_{AJ}\delta(\vec{x}) = 0. \tag{B4}$$

By means of the application of the Fourier theory and through the definition of the tensor $\hat{K}(\vec{\omega})$ with components $K_{JM}(\vec{\omega}) = \omega_i\Lambda_{iJMn}\omega_n$, we can find the following expression for the Green function:[61]

$$G_{MA}(\vec{x}) = \frac{1}{8\pi^2}\int_0^{2\pi}\int_0^{\pi}[\hat{K}^{-1}(\vec{n})]_{MA}\delta(\vec{n}\cdot\vec{x})\sin\vartheta\, d\vartheta\, d\varphi, \tag{B5}$$

where $\vec{n} = (\cos\varphi\sin\vartheta, \sin\varphi\sin\vartheta, \cos\vartheta)$. Using Eq. (B5), we can find the effects induced by an arbitrary eigenfield through the standard convolution integral:

$$\begin{aligned} U_M(\vec{x}) &= \int_{\Re^3} G_{MA}(\vec{x} - \vec{x}')b^*_A(\vec{x}')d\vec{x}' \\ &= -\int_{\Re^3} G_{MA}(\vec{x} - \vec{x}')\Lambda_{iAHn}\frac{\partial Z^*_{Hn}(\vec{x}')}{\partial x'_i}d\vec{x}' \\ &= \int_{\Re^3}\frac{\partial G_{MA}(\vec{x} - \vec{x}')}{\partial x'_i}\Lambda_{iAHn}Z^*_{Hn}(\vec{x}')d\vec{x}' \\ &= -\int_{\Re^3}\frac{\partial G_{MA}(\vec{x} - \vec{x}')}{\partial x_i}\Lambda_{iAHn}Z^*_{Hn}(\vec{x}')d\vec{x}'. \end{aligned} \tag{B6}$$

Furthermore, if the eigenstrain is uniform in a given region V (the so-called inclusion), we have

$$U_M(\vec{x}) = -\Lambda_{iAHn} Z^*_{Hn} \int_V \frac{\partial G_{MA}(\vec{x}-\vec{x}')}{\partial x_i} d\vec{x}'. \quad \text{(B7)}$$

The Eshelby theory (originally developed for the uncoupled elastic case)[62] concerns the determination of the electroelastic fields within an ellipsoidal inclusion with a given eigenfield. Therefore we have to apply Eq. (B7) to the specific case with $V = \{\vec{x} \in \Re^3 : \sum_{i=1}^3 x_i^2/a_i^2 \leqslant 1\}$. Substituting Eq. (B5) in Eq. (B7), we need the following integral:[61]

$$I(\vec{x}) = \int_V \delta[\vec{n}\cdot(\vec{x}-\vec{x}')]\vec{x}' = \frac{\pi a_1 a_2 a_3}{a^3}[a^2 - (\vec{n}\cdot\vec{x})^2] \quad \text{(B8)}$$

holding on if $\vec{x} \in V$; in Eq. (B8), we have defined the quantity $a = \sqrt{(a_1 n_1)^2 + (a_2 n_2)^2 + (a_3 n_3)^2}$. After straightforward calculations, we have

$$U_M(\vec{x}) = \Lambda_{iAHn} Z^*_{Hn} \frac{a_1 a_2 a_3}{4\pi} \times \int_0^{2\pi}\int_0^{\pi} [\hat{K}^{-1}(\vec{n})]_{MA} \frac{n_i n_j}{a^3} \sin\vartheta d\vartheta d\varphi x_j \quad \text{(B9)}$$

for any $\vec{x} \in V$. We observe that the generalized potential is a linear function of the coordinates x_j. Therefore by performing the spatial derivatives, we may determine a constant quantity $\hat{Z}$ within the inclusion. We observe that $Z_{Mn} = (1/2)(\partial u_m/\partial x_n + \partial u_n/\partial x_m)$ if $M = m \leqslant 3$ and $Z_{Mn} = \partial\phi/\partial x_n$ if $M = 4$. Therefore we simply obtain a linear relation between $\hat{Z}$ and $\hat{Z}^*$:

$$Z_{Mn} = S_{MnAb} Z^*_{Ab} \quad \text{or} \quad \hat{Z} = \hat{S}\hat{Z}^*. \quad \text{(B10)}$$

The complete expressions for the Eshelby tensor $\hat{S}$ can be eventually found as[46–48]

$$S_{MjHn} = \begin{cases} \frac{1}{2}(D_{MjHn} + D_{jMHn}) & \text{if } M \leqslant 3 \\ D_{MjHn} & \text{if } M = 4 \end{cases}, \quad \text{(B11)}$$

where

$$D_{MjHn} = \frac{a_1 a_2 a_3}{4\pi} \Lambda_{iAHn} \times \int_0^{2\pi}\int_0^{\pi} \frac{1}{a^3} [\hat{K}^{-1}(\vec{n})]_{MA} n_i n_j \sin\vartheta d\vartheta d\varphi. \quad \text{(B12)}$$

APPENDIX C: AN ALTERNATIVE METHOD FOR OBTAINING THE TENSORS $\hat{C}$, $\hat{D}$, AND $\hat{F}$

We consider a piezoelectric matrix defined in Eqs. (13) and (14) and we suppose to have an eigenfield $(\hat{\varepsilon}^*, \vec{E}^*)$ defining an inclusion (ellipsoidal and uniform):

$$\hat{T} = \hat{L}_1(\hat{\varepsilon} - \hat{\varepsilon}^*) + \hat{Q}_1(\vec{E} - \vec{E}^*), \quad \text{(C1)}$$

$$\vec{D} = \hat{R}_1(\hat{\varepsilon} - \hat{\varepsilon}^*) + \hat{\epsilon}_1(\vec{E} - \vec{E}^*), \quad \text{(C2)}$$

where $\hat{R}_1 = -\hat{Q}_1^T$. We can now rewrite these expressions as follows:

$$\hat{T} = \hat{L}_1\{\hat{\varepsilon} - [\hat{\varepsilon}^* - \hat{L}_1^{-1}\hat{Q}_1(\vec{E} - \vec{E}^*)]\}, \quad \text{(C3)}$$

$$\vec{D} = \hat{\epsilon}_1\{\vec{E} - [\vec{E}^* - \hat{\epsilon}_1^{-1}\hat{R}_1(\hat{\varepsilon} - \hat{\varepsilon}^*)]\}. \quad \text{(C4)}$$

Through the definition of the uncoupled elastic[40] ($\hat{S}_\varepsilon$) and electric[41] ($\hat{S}_e$) Eshelby tensors, we have the following relations (for the points inside the inclusion):

$$\hat{\varepsilon} = \hat{S}_\varepsilon[\hat{\varepsilon}^* - \hat{L}_1^{-1}\hat{Q}_1(\vec{E} - \vec{E}^*)] = \hat{S}_\varepsilon\hat{\varepsilon}^* - \hat{\alpha}(\vec{E} - \vec{E}^*). \quad \text{(C5)}$$

$$\vec{E} = \hat{S}_e[\vec{E}^* - \hat{\epsilon}_1^{-1}\hat{R}_1(\hat{\varepsilon} - \hat{\varepsilon}^*)] = \hat{S}_e\vec{E}^* - \hat{\beta}(\hat{\varepsilon} - \hat{\varepsilon}^*), \quad \text{(C6)}$$

where

$$\hat{\alpha} = \hat{S}_\varepsilon\hat{L}_1^{-1}\hat{Q}_1, \quad \text{(C7)}$$

$$\hat{\beta} = \hat{S}_e\hat{\epsilon}_1^{-1}\hat{R}_1. \quad \text{(C8)}$$

We can solve the system given in Eqs. (C5) and (C6), eventually obtaining $\hat{\varepsilon}$ and $\vec{E}$ in the form

$$\hat{\varepsilon} = (\hat{I} - \hat{\alpha}\hat{\beta})^{-1}[(\hat{S}_\varepsilon - \hat{\alpha}\hat{\beta})\hat{\varepsilon}^* + \hat{\alpha}(\hat{I} - \hat{S}_e)\vec{E}^*], \quad \text{(C9)}$$

$$\vec{E} = (\hat{I} - \hat{\beta}\hat{\alpha})^{-1}[\hat{\beta}(\hat{I} - \hat{S}_\varepsilon)\hat{\varepsilon}^* + (\hat{S}_e - \hat{\beta}\hat{\alpha})\vec{E}^*]. \quad \text{(C10)}$$

We remark that $(\hat{\alpha}\hat{\beta})_{ijmn} = \alpha_{ijk}\beta_{kmn}$ and $(\hat{\beta}\hat{\alpha})_{in} = \alpha_{ijk}\beta_{jkn}$. We have therefore obtained the piezoelectric Eshelby tensor in terms of the uncoupled tensors:

$$\begin{bmatrix} \hat{\varepsilon} \\ \hline -\vec{E} \end{bmatrix} = \hat{S}\begin{bmatrix} \hat{\varepsilon}^* \\ \hline -\vec{E}^* \end{bmatrix} = \begin{bmatrix} \hat{S}_{\varepsilon\varepsilon} & -\hat{S}_{\varepsilon e} \\ -\hat{S}_{e\varepsilon} & \hat{S}_{ee} \end{bmatrix}\begin{bmatrix} \hat{\varepsilon}^* \\ \hline -\vec{E}^* \end{bmatrix}, \quad \text{(C11)}$$

where

$$\hat{S} = \begin{bmatrix} (\hat{I} - \hat{\alpha}\hat{\beta})^{-1}(\hat{S}_\varepsilon - \hat{\alpha}\hat{\beta}) & -(\hat{I} - \hat{\alpha}\hat{\beta})^{-1}\hat{\alpha}(\hat{I} - \hat{S}_e) \\ -(\hat{I} - \hat{\beta}\hat{\alpha})^{-1}\hat{\beta}(\hat{I} - \hat{S}_\varepsilon) & (\hat{I} - \hat{\beta}\hat{\alpha})^{-1}(\hat{S}_e - \hat{\beta}\hat{\alpha}) \end{bmatrix}. \quad \text{(C12)}$$

It is possible to prove the perfect agreement of Eq. (C12) with Eq. (B11). In general, any multiphysics Eshelby tensor can be always written through the corresponding uncoupled versions.[63–65] This alternative result is useful to get the explicit form of tensors $\hat{C}$, $\hat{D}$, and $\hat{F}$. We use the Eshelby equivalence principle stated in Sec. IV and represented in Fig. 2. The subproblem A (uniform space) is solved by the fields

$$\hat{\varepsilon}_A = \hat{\varepsilon}^\infty, \quad \text{(C13)}$$

$$\vec{E}_A = \vec{E}^\infty, \quad \text{(C14)}$$

$$\hat{T}_A = \hat{L}_1\hat{\varepsilon}^\infty + \hat{Q}_1\vec{E}^\infty, \quad \text{(C15)}$$

$$\vec{D}_A = \hat{R}_1\hat{\varepsilon}^\infty + \hat{\epsilon}_1\vec{E}^\infty. \quad \text{(C16)}$$

On the other hands, the subproblem B (inclusion) is solved by the fields [see Eqs. (C1), (C2), and (C11)]:

$$\hat{\varepsilon}_B = \hat{S}_{\varepsilon\varepsilon}\hat{\varepsilon}^* + \hat{S}_{\varepsilon e}\vec{E}^*, \quad \text{(C17)}$$

$$\vec{E}_B = \hat{S}_{e\varepsilon}\hat{\varepsilon}^* + \hat{S}_{ee}\vec{E}^*, \quad \text{(C18)}$$

$$\hat{T}_B = \hat{L}_1(\hat{S}_{\varepsilon\varepsilon}\hat{\varepsilon}^* + \hat{S}_{\varepsilon e}\vec{E}^* - \hat{\varepsilon}^*) + \hat{Q}_1(\hat{S}_{e\varepsilon}\hat{\varepsilon}^* + \hat{S}_{ee}\vec{E}^* - \vec{E}^*), \quad \text{(C19)}$$

$$\vec{D}_B = \hat{R}_1(\hat{S}_{\varepsilon\varepsilon}\hat{\varepsilon}^* + \hat{S}_{\varepsilon e}\vec{E}^* - \hat{\varepsilon}^*) + \hat{\epsilon}_1(\hat{S}_{e\varepsilon}\hat{\varepsilon}^* + \hat{S}_{ee}\vec{E}^* - \vec{E}^*). \quad \text{(C20)}$$

Summing up, the total fields within the embedded particle can be obtained as $\hat{T} = \hat{T}_A + \hat{T}_B$, $\hat{\varepsilon} = \hat{\varepsilon}_A + \hat{\varepsilon}_B$, $\vec{D} = \vec{D}_A + \vec{D}_B$, and $\vec{E} = \vec{E}_A + \vec{E}_B$. They must satisfy the constitutive relations

of the particle $\hat{T} = \hat{L}_2\{\hat{\varepsilon} - [\hat{\varepsilon}_\mu(\vec{\gamma}) - \hat{\varepsilon}_\mu(\vec{\gamma}_0)]\}$ and $\vec{D} = \hat{\epsilon}_2\vec{E}$ as stated in Eqs. (17) and (18). Therefore we obtain a set of equations for determining the eigenfields $(\hat{\varepsilon}^*, \vec{E}^*)$ as follows:

$$\hat{a}_{11}\hat{\varepsilon}^* + \hat{a}_{12}\vec{E}^* = \hat{b}_1, \tag{C21}$$

$$\hat{a}_{21}\hat{\varepsilon}^* + \hat{a}_{22}\vec{E}^* = \hat{b}_2, \tag{C22}$$

where

$$\begin{aligned} \hat{a}_{11} &= \hat{L}_1(\hat{S}_{\varepsilon\varepsilon} - \hat{I}) - \hat{L}_2\hat{S}_{\varepsilon\varepsilon} + \hat{Q}_1\hat{S}_{e\varepsilon}, \\ \hat{a}_{12} &= (\hat{L}_1 - \hat{L}_2)\hat{S}_{\varepsilon e} + \hat{Q}_1(\hat{S}_{ee} - \hat{I}), \\ \hat{b}_1 &= (\hat{L}_2 - \hat{L}_1)\hat{\varepsilon}^\infty - \hat{Q}_1\vec{E}^\infty - \hat{L}_2[\hat{\varepsilon}_\mu(\vec{\gamma}) - \hat{\varepsilon}_\mu(\vec{\gamma}_0)], \end{aligned} \tag{C23}$$

$$\begin{aligned} \hat{a}_{21} &= (\hat{\epsilon}_1 - \hat{\epsilon}_2)\hat{S}_{e\varepsilon} + \hat{R}_1(\hat{S}_{\varepsilon\varepsilon} - \hat{I}), \\ \hat{a}_{22} &= \hat{\epsilon}_1(\hat{S}_{ee} - \hat{I}) - \hat{\epsilon}_2\hat{S}_{ee} + \hat{R}_1\hat{S}_{\varepsilon e}, \\ \hat{b}_2 &= (\hat{\epsilon}_2 - \hat{\epsilon}_1)\vec{E}^\infty - \hat{R}_1\hat{\varepsilon}^\infty. \end{aligned} \tag{C24}$$

To conclude, the following expression furnishes the elastic stress inside the magnetoelastic particle

$$\begin{aligned} \hat{T} = {} & \hat{L}_1\hat{\varepsilon}^\infty + \hat{Q}_1\vec{E}^\infty + \hat{L}_1(\hat{S}_{\varepsilon\varepsilon}\hat{\varepsilon}^* + \hat{S}_{\varepsilon e}\vec{E}^* - \hat{\varepsilon}^*) \\ & + \hat{Q}_1(\hat{S}_{e\varepsilon}\hat{\varepsilon}^* + \hat{S}_{ee}\vec{E}^* - \vec{E}^*). \end{aligned} \tag{C25}$$

The procedure utilized for determining the tensors $\hat{C}$, $\hat{D}$, and $\hat{F}$ is the following: by substituting the solutions of Eqs. (C21) and (C22) in Eq. (C25) and by considering the expressions of the Eshelby tensor given in Eq. (C12), we obtain the internal stress $\hat{T} = \hat{T}(\hat{\varepsilon}^\infty, \vec{E}^\infty, \vec{\gamma})$ in the form of Eq. (25) and the identifications of tensors $\hat{C}$, $\hat{D}$, and $\hat{F}$ is straightforward. We observe that, using the properties discussed in Appendix A, we can prove that the tensor $\hat{F}$ is always symmetric, i.e., $F_{ijkh} = F_{khij}$, similarly to any elastic tensor.

*stefano.giordano@iemn.univ-lille1.fr

[1] N. A. Spaldin and M. Fiebig, Science **309**, 391 (2005).
[2] M. Fiebig, J. Phys. D: Appl. Phys. **38**, 123 (2005).
[3] W. Eerenstein, N. D. Mathur, and J. F. Scott, Nature (London) **442**, 759 (2006).
[4] R. Ramesh and N. A. Spaldin, Nat. Mater. **6**, 21 (2007).
[5] C. W. Nan, M. I. Bichurin, S. Dong, D. Viehland, and G. Srinivasan, J. Appl. Phys. **103**, 031101 (2008).
[6] Y. Wang, J. Hu, Y. Lin, and C. W. Nan, NPG Asia Mater. **2**, 61 (2010).
[7] T. Kimura, T. Goto, H. Shintani, K. Ishizaka, T. Arima, and Y. Tokura, Nature (London) **426**, 55 (2003).
[8] V. Garcia, M. Bibes, L. Bocher, S. Valencia, F. Kronast, A. Crassous, X. Moya, S. Enouz-Vedrenne, A. Gloter, D. Imhoff, C. Deranlot, N. D. Mathur, S. Fusil, K. Bouzehouane, and A. Barthélémy, Science **327**, 106 (2010).
[9] L. Colombo and S. Giordano, Rep. Prog. Phys. **74**, 116501 (2011).
[10] J. H. Huang and W. S. Kuo, J. Appl. Phys. **81**, 1378 (1997).
[11] L. Landau and E. Lifshitz, Phys. Zeitsch. der Sow. **8**, 153 (1935).
[12] T. L. Gilbert, Phys. Rev. **100**, 1243 (1955) (abstract only); IEEE Trans. Mag. **40**, 3443 (2004).
[13] J. E. Huber, N. A. Fleck, C. M. Landis, and R. M. McMeeking, J. Mech. Phys. Sol. **47**, 1663 (1999).
[14] A. Chiabrera, E. Di Zitti, F. Costa, and G. M. Bisio, J. Phys. D: Appl. Phys. **22**, 1571 (1989).
[15] S. Salahuddin and S. Datta, Appl. Phys. Lett. **90**, 093503 (2007).
[16] K. Roy, S. Bandyopadhyay, and J. Atulasimha, Appl. Phys. Lett. **99**, 063108 (2011).
[17] S. Priya and D. J. Inman, *Energy Harvesting Technologies* (Springer Science, New York, 2010).
[18] N. D'Souza, J. Atulasimha, and S. Bandyopadhyay, J. Phys. D: Appl. Phys. **44**, 265001 (2011).
[19] N. A. Pertsev and H. Kohlstedt, Nanotechnology **21**, 475202 (2010).
[20] M. Gajek, M. Bibes, S. Fusil, K. Bouzehouane, J. Fontcuberta, A. Barthélémy, and A. Fert, Nat. Mater. **6**, 296 (2007).
[21] D. Chiba, M. Sawicki, Y. Nishitani, Y. Nakatani, F. Matsukura, and H. Ohno, Nature (London) **455**, 515 (2008).
[22] D. Chiba, Y. Nakatani, F. Matsukura, and H. Ohno, Appl. Phys. Lett. **96**, 192506 (2010).
[23] Y. H. Chu, L. W. Martin, M. B. Holcomb, M. Gajek, S. J. Han, Q. He, N. Balke, C. H. Yang, D. Lee, W. Hu, Q. Zhan, P. L. Yang, A. Fraile-Rodríguez, A. Scholl, S. X. Wang, and R. Ramesh, Nat. Mater. **7**, 478 (2008).
[24] X. He, Y. Wang, N. Wu, A. N. Caruso, E. Vescovo, K. D. Belashchenko, P. A. Dowben, and C. Binek, Nat. Mater. **9**, 579 (2010).
[25] J. T. Heron, M. Trassin, K. Ashraf, M. Gajek, Q. He, S. Y. Yang, D. E. Nikonov, Y.-H. Chu, S. Salahuddin, and R. Ramesh, Phys. Rev. Lett. **107**, 217202 (2011).
[26] T. Wu, A. Bur, K. Wong, P. Zhao, C. S. Lynch, P. K. Amiri, K. L. Wang, and G. P. Carman, Appl. Phys. Lett. **98**, 262504 (2011).
[27] A. Brandlmaier, S. Geprägs, G. Woltersdorf, R. Gross, and S. T. B. Goennenwein, J. Appl. Phys. **110**, 043913 (2011).
[28] T. Brintlinger, S. H. Lim, K. H. Baloch, P. Alexander, Y. Qi, J. Barry, J. Melngailis, L. Salamanca-Riba, I. Takeuchi, and J. Cumings, Nano Lett. **10**, 1219 (2010).
[29] J. Stöhr, H. C. Siegmann, A. Kashuba, and S. J. Gamble, Appl. Phys. Lett. **94**, 072504 (2009).
[30] T. Maruyama, Y. Shiota, T. Nozaki, K. Ohta, N. Toda, M. Mizuguchi, A. A. Tulapurkar, T. Shinjo, M. Shiraishi, S. Mizukami, Y. Ando, and Y. Suzuki, Nat. Nano **4**, 158 (2009).
[31] P. Balestriere, T. Devolder, J. Wunderlich, and C. Chappert, Appl. Phys. Lett. **96**, 142504 (2010).
[32] K. Roy, S. Bandyopadhyay, and J. Atulasimha, Phys. Rev. B **83**, 224412 (2011).
[33] N. Tiercelin, Y. Dusch, V. Preobrazhensky, and P. Pernod, J. Appl. Phys. **109**, 07D726 (2011).
[34] N. Tiercelin, Y. Dusch, A. Klimov, S. Giordano, V. Preobrazhensky, and P. Pernod, Appl. Phys. Lett. **99**, 192507 (2011).
[35] N. Tiercelin, Y. Dusch, V. Preobrazhensky, and P. Pernod, Mémoire magnéto-électrique, Dépôt de brevet N. FR 10/02580, accepted on Feb. 15 (2011).
[36] J. S. Moodera, L. R. Kinder, T. M. Wong, and R. Meservey, Phys. Rev. Lett. **74**, 3273 (1995).
[37] L. Daniel, O. Hubert, N. Buiron, and R. Billardonb, J. Mech. Phys. Sol. **56**, 1018 (2008).

[38] A. Klimov, Y. Ignatov, N. Tiercelin, V. Preobrazhensky, P. Pernod, and S. Nikitov, J. Appl. Phys. **107**, 093916 (2010).
[39] F. G. West, J. Appl. Phys. **35**, 1827 (1964).
[40] S. Giordano, P. L. Palla, and L. Colombo, Europhys. Lett. **83**, 66003 (2008).
[41] S. Giordano and P. L. Palla, J. Phys. A: Math. Theor. **41**, 415205 (2008).
[42] P. L. Palla, S. Giordano, and L. Colombo, Phys. Rev. B **81**, 214113 (2010).
[43] L. D. Landau and E. M. Lifshitz, *Electrodynamics of Continuous Media* (Pergamon Press, London, 1984).
[44] S. Giordano, J. Electrost. **58**, 59 (2003).
[45] H. Suhl, *Relaxation Processes in Micromagnetics* (Oxford University Press, New York, 2007).
[46] J. H. Huang, Y. H. Chiu, and H. K. Liu, J. Appl. Phys. **83**, 5364 (1998).
[47] Y. Mikata, Int. J. Sol. Struct. **38**, 7045 (2001).
[48] J. Y. Li and M. L. Dunn, Phil. Mag. A **77**, 1341 (1998).
[49] P. L. Palla, S. Giordano, and L. Colombo, Phys. Rev. B **78**, 012105 (2008).
[50] P. L. Palla, S. Giordano, and L. Colombo, Phys. Rev. B **80**, 054105 (2009).
[51] S. Giordano, P. L. Palla, E. Cadelano, and M. Brun, Mech. Mat. **44**, 4 (2012).
[52] G. Dewar, J. Appl. Phys. **81**, 5713 (1997).
[53] Y. Y. Huang and Y. M. Jin, Appl. Phys. Lett. **93**, 142504 (2008).
[54] T. Kobayashi, H. Hayashi, Y. Fujiwara, and S. Shiomi, Magnetics Conference, 2005. INTERMAG Asia 2005. Digests of the IEEE International, 253 (2005).
[55] M. H. Kryder and C. S. Kim, IEEE Trans. Magn. **45**, 3406 (2009).
[56] W. F. Brown, Phys. Rev. **130**, 1677 (1963).
[57] D. A. Garanin, Phys. Rev. B **55**, 3050 (1997).
[58] B. Lambson, D. Carlton, and J. Bokor, Phys. Rev. Lett. **107**, 010604 (2011).
[59] J. A. Stratton, *Electromagnetic Theory* (Mc Graw Hill, New York, 1941).
[60] A. E. H. Love, *A Treatise on the Mathematical Theory of Elasticity* (Dover, New York, 2002).
[61] T. Mura, *Micromechanics of Defects in Solids* (Kluwer, Dordrecht, 1987).
[62] J. D. Eshelby, Proc. R. Soc. London A **241**, 376 (1957).
[63] R. Corcolle, L. Daniel, and F. Bouillault, Phys. Rev. B **78**, 214110 (2008).
[64] J. Bing, F. Daining, and H. Kehchih, Acta Mechanica Sinica **13**, 339 (1997); **13**, 347 (1997).
[65] X. Feng, D. N. Fang, and K. C. Hwang, Eur. J. Mech. A/Solids **23**, 1007 (2004).